# Nonlinear dynamics of microcantilevers in tapping mode atomic force microscopy: A comparison between theory and experiment

S. I. Lee,[1] S. W. Howell,[2] A. Raman,[1] and R. Reifenberger[2]
[1]*School of Mechanical Engineering, Purdue University, West Lafayette, Indiana 47907*
[2]*Department of Physics, Purdue University, West Lafayette, Indiana 47907*
(Received 5 June 2002; published 17 September 2002)

The nonlinear dynamic response of atomic force microscopy cantilevers tapping on a sample is discussed through theoretical, computational, and experimental analysis. Experimental measurements are presented for the frequency response of a specific microcantilever-sample system to demonstrate the nonlinear features, including multiple jump phenomena leading to reproducible hysteresis. We show that a comprehensive analysis using modern continuation tools for computational nonlinear dynamics and bifurcation problems reproduces all essential features of the data. A close connection is established between the features of the interaction potential well and the nonlinear forced tip response. In particular, the effects of the nonlinear van der Waals forces, the nanoscale contact nonlinearities, and microcantilever damping, as well as the effects of forced and parametric excitation on the bifurcations and instabilities of forced periodic motions of the microcantilever system, are discussed in detail. The results indicate that nonlinear system identification methods could be used as effective tools to extract detailed information about the tip–surface interaction potential.

DOI: 10.1103/PhysRevB.66.115409 PACS number(s): 68.35.Ja, 05.45.−a, 68.37.Ps

## I. INTRODUCTION

Atomic force microscopy (AFM) with tapping (or intermittent contact) mode operation has been widely used in scanning probe studies as a method to reduce damage to soft substrates.[1,2] Early studies of this imaging mode with the tip in close proximity to the surface have shown an interesting ''bistable'' behavior in which both the tip amplitude and the phase show reproducible hysteresis as the driving frequency is swept up and down through resonance.[3] This phenomenon was explained as a result of the interaction of a harmonic oscillator with the attractive and the repulsive regions of the interaction potential. It was recognized that these unusual dynamics would cause unpredictable behavior while imaging. Attempts to further understand this behavior have been reported by including a single degree-of-freedom oscillator model along with different nonlinear contact models and van der Waals forces.[1,4–11] Of particular interest in this context is the role played by nonlinear van der Waals, nanoscale contact, and capillary forces between the tip and the sample in controlling this bistable behavior.[12] The influence of van der Waals forces was recognized and imaging artifacts such as strange contours and unexpected height shifts due to nonlinear dynamic instabilities were also reported.[1,4] The effects of the nonlinear van der Waals forces on the dynamic response in noncontact dynamic force microscopy have been reported.[10,11] Nonlinear hysteresis and jumps in the dynamic response were examined as the tip approaches and retracts from the sample at a fixed excitation frequency.[13,14] The nonlinear dynamic response to frequency sweeps in the tapping mode was simulated using van der Waals attractive forces and the Derjaguin-Muller-Toporov (DMT) and Johnson-Kendall-Roberts (JKR) contact models.[2,15] The nonlinear effects in the dynamic response of a simple oscillator model were examined through numerical simulations of frequency sweeps.[9]

While this prior work has done much to demonstrate the occurrence of the bistable behavior and describe the parameters that affect it, the prior work is based primarily on numerical simulations of the equations of motion. While stable periodic responses are easily followed using numerical simulations, their stability and the presence of unstable periodic motions have not been computed so that the mechanisms of instability have not been described clearly. A few analytical works[10,11,15,16] on the subject deal mostly with approximate solutions based on variants of the multiple scale or the averaging method,[17] and they are restricted to noncontact models that include only the van der Waals forces. These approximate techniques are valid only for weakly nonlinear systems and are thus unsuitable for the study of the strongly nonlinear tapping mode. Moreover, the existing literature has mostly modeled the piezo forcing as an external excitation term. As will be shown in this paper, the base excitation of the microcantilever leads to complex linear and nonlinear parametric excitation terms in addition to an external forcing term. This can lead to significantly different stability results, especially for vacuum AFM applications. Finally, a rational connection between certain features of the tip-sample interaction potential and the nonlinear response has not been established satisfactorily. A comprehensive nonlinear analysis of the tapping mode AFM using the dynamically correct excitation terms and using computational continuation tools has not yet been presented. Such tools are ideally suited for the study of strongly nonlinear systems and allow for convenient continuation of stable and unstable forced periodic solutions, and the detection of complex bifurcations including folds, period doublings, and torus bifurcations.

To address this problem, we have combined both experimental and nonlinear continuation analysis of a tapping mode AFM microcantilever including all the dynamically exact excitation terms. In the experimental analysis, the tip amplitude and phase were measured using a diving-board cantilever, a silicon tip, and a freshly cleaved HOPG (highly oriented pyrolytic graphite) sample. Experimental data show highly nonlinear dynamic phenomena including jumps in amplitude and phase response. In the computational analysis,

 

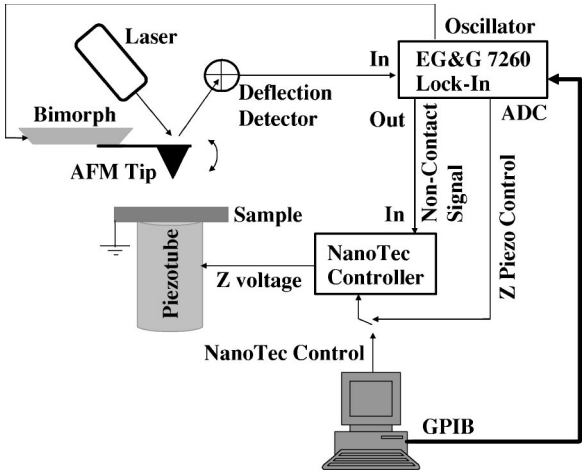


FIG. 1. A schematic diagram of the experimental setup for measuring the nonlinear behavior near resonance of microcantilevers interacting with samples.

a discretized model of the AFM microcantilever with long-range attractive van der Waals force and DMT contact mechanics are used to model the tip–surface interactions including adhesion, as well as sample deformation during tip-sample contact. Computational analysis of this model using continuation techniques reveal the bifurcations and the effects of the excitation terms explicitly without *a priori* approximation of the solution form. We show that this approach enables a comprehensive understanding of the nonlinear dynamic behavior observed in the AFM experiments. Moreover, a detailed discussion of the free oscillations of the system as well as of the exact excitation terms are used to explain the close connection between the characteristics of the potential well and the microcantilever response. This suggests that nonlinear system identification techniques may be used effectively for systematic measurement of the interaction potential between various tip-sample combinations.[16]

## II. EXPERIMENT

To demonstrate the effects of nonlinearities on the AFM tip response, a commercially available air AFM produced by NanoTec™ was chosen to perform these experiments. An Olympus™ diving-board silicon cantilever (resonance frequency 44 kHz, $Q \approx 33$) was employed. The experimental setup is displayed in Fig. 1. In order to perform experiments on the nonlinear response of the cantilever, it is necessary to have control of the tip-sample separation as the frequency of excitation is systematically varied. The amplitude and phase of the cantilever response must be rapidly measured as a function of the excitation frequency. In general, this is difficult to achieve in commercial scanning probe systems and requires the use of a flexible software system. In our case, we used the $WS \times M$ software available from NanoTec™.

The standard AFM control system is used to bring the tip to a distance $\sim 200$ nm above the sample while operating the AFM in noncontact mode. After the initial coarse approach, the frequency response of the cantilever is measured systematically as a function of decreasing tip-sample separation. This is accomplished by rerouting the control of the $Z$ segment of the AFM's piezotube to a digital-to-analog converter (DAC) onboard the lock-in amplifier. The DAC provides the voltage required to control the $Z$ expansion of the piezotube. The expansion of the piezotube as well as the driving frequency of the cantilever are controlled by the lock-in via a general-purpose interface bus (GPIB) controller. The GPIB software controls the voltage step applied to the high-voltage power supply of the piezotube, the frequency used to drive the cantilever, and the measurement of the cantilever oscillation. The GPIB code runs on a 233-MHz Pentium PC simultaneously and independently of the NanoTec™ software.

At each tip-sample separation, the excitation frequency $\Omega$ is increased from a starting frequency to a final frequency ($\Omega_i \rightarrow \Omega_f$) across microcantilever's linear resonance frequency $\omega_1$. Then the frequency is decreased across resonance from $\Omega_f$ to $\Omega_i$. For each frequency increment ($\Delta f = 40$ Hz), the amplitude and phase of the cantilever oscillation referenced to the excitation frequency are measured by the lock-in amplifier.

In addition, an onboard analog-to-digital converter is used to measure the static force-deflection curve of the cantilever at each $Z$ step. As the tip-sample separation decreases, the tip jumps into contact with the sample when the surface forces overcome the restoring force of the cantilever. The distance from the starting position of the sample to the jump to contact point provides an initial estimate of the tip-sample separation. A better estimate of this quantity was obtained by taking into account the distance that the cantilever moved in the $z$ direction during the jump to contact. This quantity is measured by moving the sample past the jump to contact point until the cantilever returns to its unperturbed (nondeflected) position. By combining these two values, a reasonably accurate estimate of the tip-sample separation can be achieved.

Following this approach, the tip-sample separation is reduced in increments until the cantilever oscillation displays nonlinear resonance behavior, indicating that the tip is tapping the sample. By plotting the amplitude and phase response of the cantilever as a function of $Z$, it is possible to map out the entire nonlinear response of the cantilever.

Representative data obtained following this procedure are shown in Fig. 2 that shows the resonant response in air when (i) the tip is far away from the sample and (ii) the tip-sample separation is $\sim 90$ nm. The excitation level of the dither piezoactuator is identical in both cases. Discontinuities in the amplitude and phase at specific driving frequencies can be observed in Fig. 2. Finite jumps occur on and off a ''saturated'' amplitude branch. The cantilever response on this branch is highly nonlinear with higher harmonics of the excitation present in the response as the tip impacts the sample. The jumps render hysteretic the response of the cantilever when the driving frequency is swept up and down. In the inset in Fig. 2, a small amplitude difference of the saturated branch is observed during frequency sweep up and down, and is attributed to thermal $Z$ drift.

Experimentally, it is important to measure accurately the frequency at which the finite jumps in amplitude occur, the

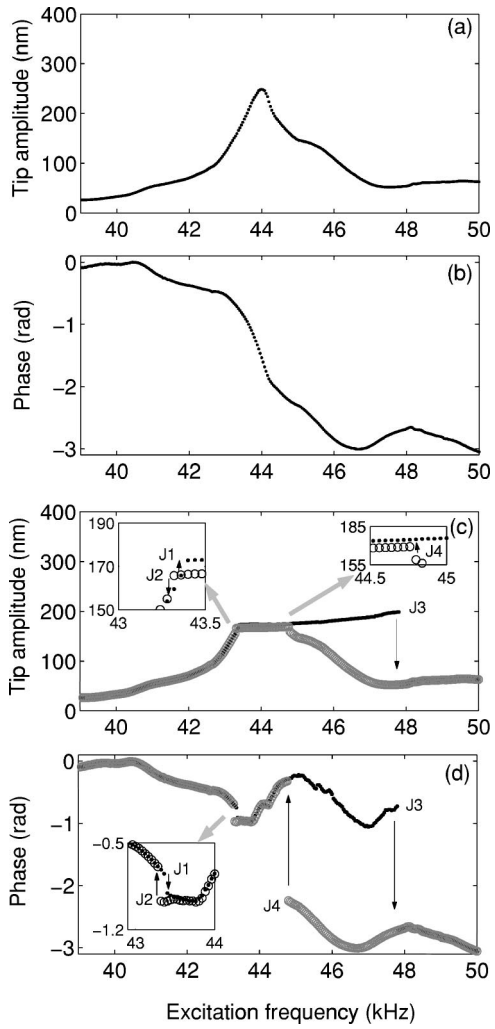


FIG. 2. Peak-to-peak amplitude and phase (with respect to driving frequency) of the silicon tip on HOPG sample. Linear tip amplitude (a) and phase (b) response when tip is far from sample ($Z > 200$ nm). Nonlinear tip amplitude (c) and phase (d) response with 90-nm tip-sample separation. Circles: response during frequency sweep up; Dots: response during frequency sweep down. The arrows indicate the abrupt discontinuities in amplitude and phase that are important signatures of the nonlinear interaction potential. Tip amplitude indicates the peak-to-peak tip oscillation amplitude of the microcantilever.

extent of the observed hysteresis, as well as the extent of the saturated response of the cantilever. These quantities are directly related to tip–surface interaction parameters that are of considerable interest. As will be discussed below, all of these nonlinear features can be explained by a complete computational nonlinear dynamic analysis, and can provide important information about the tip-sample interaction potential.

## III. TIP-SAMPLE INTERACTION MODEL AND EQUATION OF MOTION

### A. Tip-sample interaction and nonlinear static equilibrium

To analyze the tip-sample interaction in tapping mode AFM, van der Waals and DMT contact[18] forces ($F_{vdW}$, $F_{DMT}$) between a sphere (tip apex) and a flat surface (sample) are assumed. Other interaction models can be easily incorporated to characterize more accurately the specific physics of the interaction. For this sphere-flat surface geometry, the forces are[2]

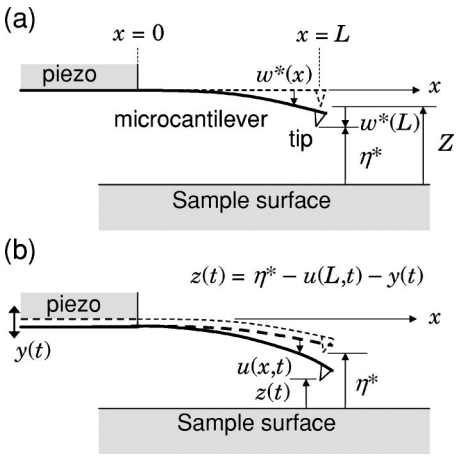


FIG. 3. Schematic diagram of the cantilever configurations. (a) Initial statically deflected configuration under van der Waals tip forces. $Z$ is the tip-sample separation in the absence of van der Waals forces. (b) Dynamic (current) configuration as cantilever vibrates about its elastostatic equilibrium.

$$F_{vdW}(z) = -\frac{AR}{6z^2} \quad \text{for} \quad z > a_0 \tag{1}$$

$$F_{DMT}(z) = -\frac{AR}{6a_0^2} + \frac{4}{3}E^*\sqrt{R}(a_0 - z)^{3/2} \quad \text{for} \quad z \leqslant a_0 \tag{2}$$

where $A$ is the Hamaker constant, $R$ is the tip radius, $z$ is the instantaneous tip-sample separation (Fig. 3), $a_0$ is the intermolecular distance[2] at which contact is initiated, and $E^*$ the effective elastic modulus of tip and sample. Figure 4 shows

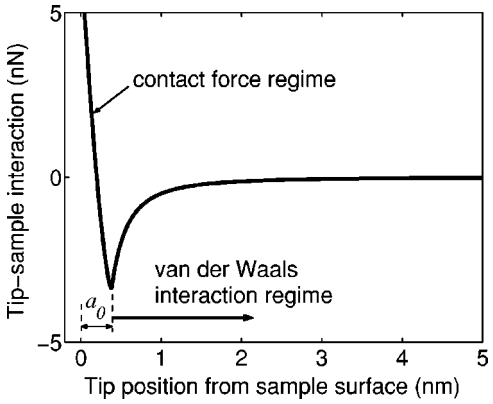


FIG. 4. Interaction model described by van der Waals and DMT contact forces. The interaction can be divided into two regimes: van der Waals force regime [Eq. (1)] and DMT contact regime [Eq. (2)]. Negative interaction implies attractive force, whereas positive interaction in contact regime represents repulsive or elastic restoring force.

TABLE I. Used constants and properties of the Si microcantilever and HOPG sample in numerical computation.

| Description | Value |
|---|---|
| Tip radius | $R=10$ nm |
| Cantilever cross-section area | $A_c=8.09\times10^{-11}$ m$^2$ |
| Cantilever area moment | $I_c=3.57\times10^{-23}$ m$^4$ |
| Cantilever material density | $\rho_c=2300$ kg/m$^3$ |
| Cantilever Young's modulus | $E_c=130$ GPa |
| Effective elastic modulus | $E^*=10.2$ GPa |
| Static bending stiffness | $k=0.87$ N/m |
| First natural frequency | $f_1=44.0$ kHz |
| $Q$ factor (in air) | $Q=33.3$ |
| Hamaker constant (Si-HOPG) | $A=2.96\times10^{-19}$ J |
| Intermolecular distance | $a_0=3.8$ Å |

the tip-sample interaction described by van der Waals and DMT contact forces in Eqs. (1) and (2) with the values listed in Table I.

All the key system parameters needed for the static equilibria as well as for the nonlinear dynamics computations are listed in Table I. Some of system parameters listed in Table I are obtained from the linear vibration experiments performed far from the sample, while other properties are taken from the literature. Resonance frequency $f_1$ and $Q$ factor are obtained from the experimental frequency response of the microcantilever without sample. The tip radius $R$, cantilever stiffness $k$, cantilever cross-section area $A_c$, and area moment $I_c$ are taken from the manufacturer's catalog (http://www.olympus.co.jp) of the microcantilever (OMCL-AC240TS) used in the experiment. Cantilever material density $\rho_c$, Young's modulus $E_c$, and effective elastic modulus $E^*$ are based on typical values for silicon and graphite using Poisson's ratio of 0.3.[12] The Hamaker constant $A$ between Si and HOPG is derived from the values of silicon-air and graphite-air Hamaker constants, which are found in the literature.[19] Finally, the intermolecular distance $a_0$ is calculated from the force equilibrium between the silicon-graphite surface force and van der Waals force.[2] It may be emphasized here that none of the chosen parameter values used for the computation are fitted to match the nonlinear experimental data.

Static equilibrium of the microcantilever without dynamic excitation is computed by solving the nonlinear elastostatic problem of the steady deflection towards the sample [$w^*(x)$ in Fig. 3(a)] of the microcantilever interacting with a nonlinear deflection-dependent forces (Fig. 4). Let $Z$ be the gap between the sample and probe tip in the reference configuration (see Fig. 3). Following the Bernoulli-Euler beam theory for infinitesimal deflections $w^*(x)$ is given by

$$E_c I_c w^{*\prime\prime\prime\prime}(x)=F_i(Z-w^*(L))\,\delta(x-L), \tag{3}$$

where a prime indicates derivative with respect to $x$, and $F_i$ is the total tip-sample interaction forces combined by $F_{vdW}$ [Eq. (1)] and $F_{DMT}$ [Eq. (2)]. Solving Eq. (3) for different $Z$ yields the equilibrium gap between the tip and sample, $\eta^*=Z-w^*(L)$, as a function of $Z$. The Liapunov stability of an equilibrium is computed easily using the Lagrange-Dirichlét theorem.[20]

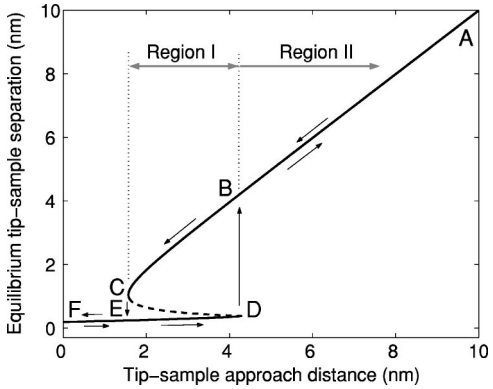


FIG. 5. Equilibrium solutions of the nonlinear equilibrium and their stability. The solid lines represent Liapunov stable solutions while the dashed line indicates an unstable equilibrium. Tip-sample approach: $A\rightarrow B\rightarrow$ C $\rightarrow E\rightarrow F$. Tip-sample retract: $F\rightarrow E\rightarrow D\rightarrow B\rightarrow A$.

Figure 5 shows the equilibrium solutions for the tip deflection and their stability. For the nonlinear equilibrium solutions, we use the values listed in Table I. As the tip is brought closer to the surface (as $Z$ decreases), the tip-sample gap decreases until point $C$ in Fig. 5 when the tip snaps into the sample ($C\rightarrow E$). As the microcantilever is pulled off from the surface, it snaps out of the surface from $D$ to $B$ in Fig. 5. These phenomena are the well-known AFM microcantilever instabilities that are caused by the transition between the *bistable* region (region I in Fig. 5) and the *monostable* region (region II in Fig. 5).

The dynamics of the microcantilever in Region I and II are significantly different with distinct nonlinear behaviors and unique instability mechanisms. This is illustrated in Fig. 6 where the potential wells are plotted for $Z=2.0$ nm and $Z=5.0$ nm corresponding, respectively, to regions I and II. Additionally, the corresponding phase portraits of free oscil-

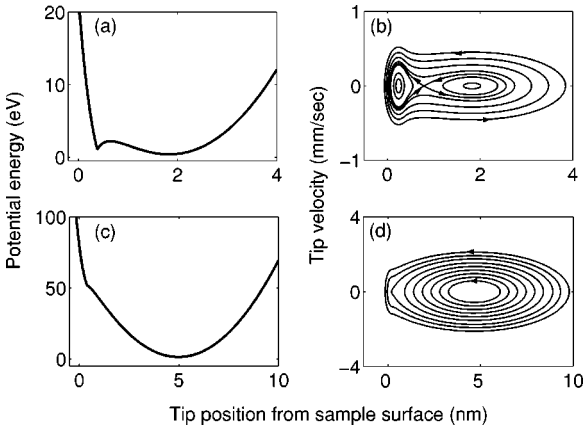


FIG. 6. Potential energy curves and their phase portraits: (a), and (b) show asymmetric two-well potential in region I (at $Z=2.0$ nm); (c) and (d) show single-well potential with contact in region II (at $Z=5.0$ nm).

lations associated with different initial energy levels are shown in Fig. 6. This requires the use of the single degree-of-freedom model of the cantilever, which is developed in the following sections; however, the phase portraits are shown to demonstrate the qualitative difference in the dynamics in regions I and II. The potential energy is an asymmetric two-well potential in region I [Figs. 6(a) and 6(b)], while it is a single-well potential in region II [Figs. 6(c) and 6(d)]. In both cases the tip-sample contact leads to nonsmoothness of the potential well. The presence of the two-well potential in region II leads to the presence of two homoclinic orbits connected at an unstable saddle located between the two equilibria. The equilibrium closer to the sample corresponds to a state where the tip is effectively stuck to the sample. Note also that the forced vibration responses of the tip in these two potential wells are expected to be very different. However, for sharp AFM tips the $Z$ range for region I is very small. In general, therefore, the practical operating regime in tapping mode AFM is region II. Hence our investigations in this paper for the tapping mode dynamics of AFM microcantilever are focused on region II.

### B. Equation for microcantilever dynamics

Consider the total dynamic deflection of the beam towards the sample

$$w(x,t)=u(x,t)+w^*(x)+y(t),$$

where $u(x,t)$ is the cantilever deflection relative to a noninertial frame attached to the moving base [Fig. 3(b)]. The excitation from the dither piezoelectric actuator is modeled as a base, harmonic motion $y(t)$ towards the sample with frequency $\Omega$, i.e., $y(t)=Y\sin\Omega t$. Writing the equations of motion of the vibrating microcantilever in a *noninertial reference frame* attached to the base of the microcantilever leads to the following representation of the vibrations about the equilibrium:

$$\rho_c A_c \ddot{u}(x,t)+E_c I_c[u'''' (x,t)+w^{*\prime\prime\prime\prime}(x)] = F_i[Z-w(L,t)]\delta(x-L)+\rho_c A_c \Omega^2 Y\sin\Omega t. \quad (4)$$

Equation (4) is highly nonlinear and nonautonomous, and its discretization may be achieved suitably through a projection of the dynamics onto the linear modes of the system. However, the linear modes and frequencies of the microcantilever about its static equilibrium are different from those of a microcantilever located far from the sample surface.[21] Using Galerkin's method,[22] the linear modes and frequencies of the microcantilever about the chosen nonlinear equilibrium (a specific position on the stable equilibrium solution in Fig. 5) are computed and lead to the approximate eigenfunction solutions.

Consider now the situation when the excitation frequency $\Omega$ in Eq. (4) is close to the lowest natural frequency $\omega_1$ of the microcantilever about its elastostatic equilibrium. Under near-resonant forcing, only one mode of the microcantilever is assumed to participate in the response:

$$u(x,t)=\Phi_1(x)q_1(t), \quad (5)$$

where $\Phi_1(x)$ is the first approximate eigenfunction of the cantilever[23] about the chosen equilibrium and $q_1(t)$ is the time-dependent generalized coordinate. Substitution of Eq. (5) into Eq. (4), and on taking inner products of the resulting equations with $\Phi_1(x)$ yields the suitably discretized dimensionless ordinary differential equation of motion of the AFM tip:

$$\frac{d^2\bar{\eta}}{d\tau^2}+D\frac{d\bar{\eta}}{d\tau}+\bar{\eta}=-C_1+\bar{F}_i(\bar{z})+B\bar{\Omega}^2\bar{y}\sin\bar{\Omega}\tau, \quad (6)$$

where

$$\bar{\eta}=\frac{u(L,\tau)}{\eta^*},\quad \bar{y}=\frac{Y}{\eta^*},\quad \bar{\Omega}=\frac{\Omega}{\omega_1},\quad \tau=\omega_1 t,$$

$$D=\frac{1}{Q},\quad B=\frac{\Phi_1(L)\int_0^L\Phi_1 dx}{\int_0^L\Phi_1^2 dx},$$

$$C_1=-\frac{AR\Phi_1^2(L)}{6(\eta^*)^3\omega_1^2\rho_c A_c\int_0^L\Phi_1^2 dx},$$

$$\bar{F}_i(\bar{z})=\begin{cases} C_1/\bar{z}^2, & \text{for}\quad \bar{z}>\bar{a}_0 \\ C_1/(\bar{a}_0^2)+C_2(\bar{a}_0-\bar{z})^{3/2} & \text{for}\quad \bar{z}\le\bar{a}_0, \end{cases}$$

$$C_2=\frac{4E^*\sqrt{R\eta^*}\Phi_1^2(L)}{3\omega_1^2\rho_c A_c\int_0^L\Phi_1^2 dx},$$

$$\bar{z}=1-\bar{\eta}(\tau)-\bar{y}\sin\bar{\Omega}\tau,\quad \text{and}\quad \bar{a}_0=\frac{a_0}{\eta^*}.$$

Note that because Eq. (6) contains explicitly time-dependent terms in $\bar{F}_i$, it is more accurate than the models investigated in earlier works.[1–6,9,15]

## IV. COMPUTATIONAL RESULTS AND DISCUSSION

For the system under consideration, we use the values listed in Table I. Use of these parameter values yields the nondimensionalized, discretized model [Eq. (6)] of the single mode response about the chosen equilibrium (at $Z=90$ nm) with specific coefficients:[24] $D=0.03$, $C_1=7.550\,57\times10^{-7}$, $C_2=4.552\,25\times10^2$, $B=1.565\,98$, and $\bar{y}=0.020\,90$.

### A. Free nonlinear oscillations

First consider the unforced, undamped vibrations of the system [Eq. (6)], $D=\bar{y}=0$ with different initial conditions corresponding to $(d/d\tau)\bar{\eta}(0)=0$ and increasing initial displacements $\bar{\eta}(0)=\bar{\eta}_0$. The resulting free oscillations correspond to different level sets of the Hamiltonian of the integrable system. These free oscillations are simulated in

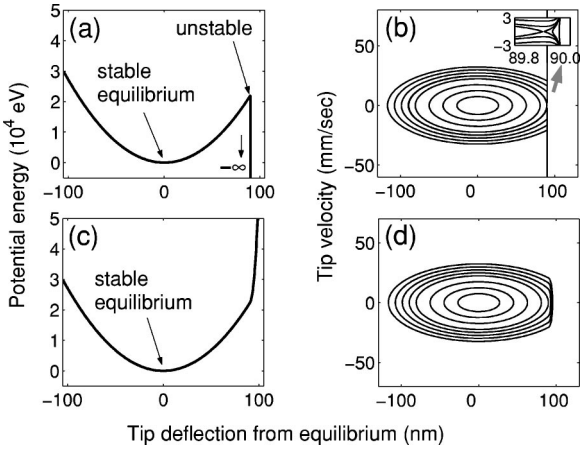


FIG. 7. Total potential energy wells and the corresponding phase portraits (a), (b) with only van der Waals forces, and (c), (d) with DMT contact included. In both cases, tip-sample separation $Z = 90$ nm (in region II). The inset in (b) shows the unstable equilibrium point in (a) is a saddle point in phase space.

MATLAB and characterized by plots of the potential well and phase portraits as a function of initial tip displacement in Fig. 7. While the free oscillations contain higher harmonics, the fundamental frequency of the resulting periodic oscillations can also be extracted. It is useful to plot the initial displacement as a function of the frequency shift parameter that specifies the change in frequency from the linear resonance frequency and the initial displacement in Figs. 7 and 8 for two cases, namely (i) when only van der Waals forces are present and (ii) when the DMT contact interactions are also included in the model. These loci of the variation of *nonlinear* frequency shift with increasing tip oscillation amplitude are referred to as ''backbone'' curves[17] and are intimately connected to the shape of the potential well in which the AFM tip oscillates.

In Figs. 7(a), (b) and 8(a), the potential well, phase portrait, and the corresponding backbone curve for case (i) clearly demonstrate that the van der Waals forces cause a softening nonlinear response.[17] This arises in Fig. 8(a) because the potential well exhibits two local minima and one local maximum corresponding to a pair of stable equilibria

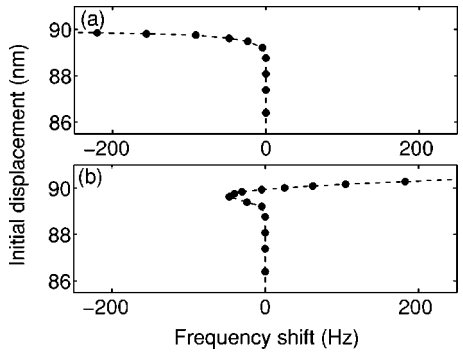


FIG. 8. The backbone curves (nonlinear resonance) (a) with only van der Waals forces [corresponding to Fig. 7(a)], and (b) with DMT contact included [corresponding to Fig. 7(c)]. In both cases, tip-sample separation $Z = 90$ nm (in region II).

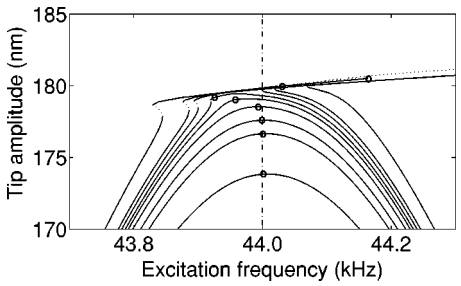


FIG. 9. Near-resonant forced responses with the different base excitation amplitude $\bar{y}$ (or $Y$) using AUTO at $Z = 90$ nm. Solid/dotted lines indicate stable/unstable solutions, respectively. Encircled points indicate the resonance points of the nonlinear forced responses. The locus of such points follows the backbone curve. The vertical dash-dotted line shows the linear natural frequency when the tip is very far from the surface. Tip amplitude indicates the peak-to-peak tip oscillation amplitude of the microcantilever.

and one unstable equilibrium. As initial displacements are increased from the stable equilibrium, the natural frequencies decrease and eventually reach zero when the initial conditions place the tip exactly on the unstable saddle [see the inset in Fig. 7(b)].

Figures 7(c), (d) and 8(b) demonstrate the case (ii) wherein the backbone curve displays an initial softening nonlinearity and for larger amplitudes the response hardens as the tip taps the sample during its free oscillations. Even in the presence of the DMT contact interaction, the resulting potential well [Fig. 8(b)] is a single well, asymmetric potential that always exhibits an eventually hardening nonlinear response. Understanding the backbone curves and their relationship to the potential wells is critical because the forced vibration response near resonance of the AFM tip follows similar trends.

### B. Forced vibration response

Next, consider the forced, damped vibrations of the system [Eq. (6)], which are the real tapping mode responses in AFM. Equation (6) represents a highly nonlinear, nonsmooth dynamical system with simultaneous external and parametric forcing. The continuation and stability characterization of forced periodic solutions when $\bar{y} > 0$ are conveniently performed using AUTO97.[25] AUTO97 uses sophisticated pseudo-arc length continuation and accurate Floquet multiplier calculations to follow both stable and unstable periodic solutions and also identify their bifurcations of periodic solutions. The response often contains higher harmonics and the phase of the response with respect to the excitation is then computed using the first harmonic of the response. To avoid mathematical complications due to nonsmoothness at $z = a_0$ in AUTO computations, we use a smooth, cubic interpolation in a thin ''boundary'' layer about $z = a_0$. Further, the AUTO computations are validated using MATLAB-based simulations. In what follows, stable and unstable periodic solutions are denoted, respectively, by solid and dotted lines.

Using AUTO, the forced responses of the model when the tip is near tapping the surface are plotted in Fig. 9 with fixed

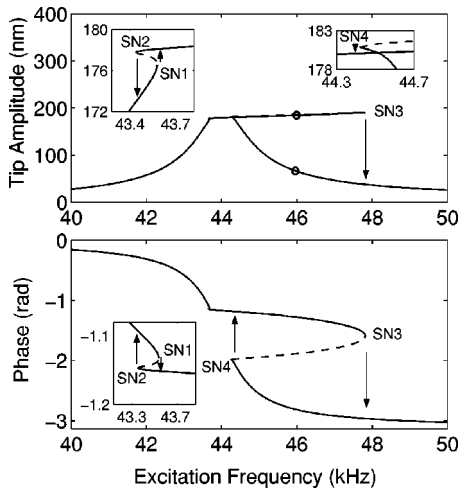


FIG. 10. Tapping mode response prediction using periodic solution continuation and stability routines in AUTO. Solid/dotted lines indicate stable/unstable solutions, respectively. Tip amplitude indicates the peak-to-peak tip oscillation amplitude of the microcantilever. Phase between the first harmonic of response and the base excitation is computed in AUTO.

$Z=90$ nm, while the amplitude of base excitation $\bar{y}$ is increased with the values of 0.0185, 0.0191, 0.0193, 0.0195, 0.0196, 0.0197, 0.0198, 0.0199, 0.0200, and 0.0205. The resonance points on the forced response diagram corresponding to a $\pi/2$ phase lag with respect to forcing of the first harmonic of the response are shown with a circle for each $\bar{y}$. This result shows that with increasing amplitude of excitation the locus of the resonance points follows the backbone curve [Fig. 8(b)] generated for the free oscillations of the system. Therefore, the initial softening and subsequent hardening in forced nonlinear response mirrors the behavior of the backbone curve.

### C. Comparison of theory and experiment

For the specific value of $\bar{y}=0.020\,90$ chosen in the experiment, the computational solution using AUTO of the amplitude and phase (of the first harmonic of motion with respect to base motion) is plotted in Fig. 10. This is to be compared to the experimental response in Fig. 2. The computational results reproduce very closely the experimentally observed response (Fig. 2). As the frequency is increased from below resonance, the computed periodic solution follows the stable branch and jumps into another stable branch at SN1 and SN3 in Fig. 10, where SN stands for saddle node. Likewise, during a frequency sweep up, the experimentally measured response in Fig. 2 follows the solid dots leading to jumps at $J1$ and $J3$. Similarly the computed response during a decrease of excitation frequency from above resonance jumps at SN4 and SN2 (Fig. 10) and the experimentally measured response during frequency sweep down (circles in Fig. 2) encounters jumps at $J4$ and $J2$.

The response in Fig. 10 also follows the backbone curve in Fig. 8(b). The initial softening and subsequent hardening of the forced vibration response then leads to the occurrence

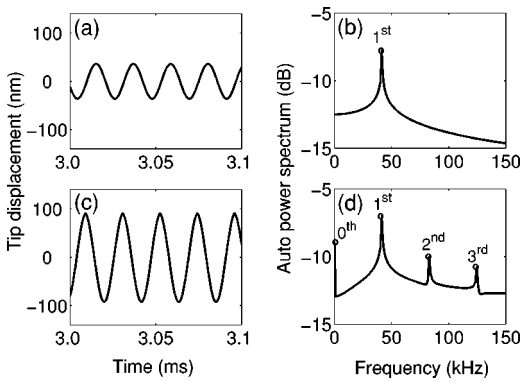


FIG. 11. Tip displacement response about the elastostatic equilibrium when the external forcing frequency is at 46.0 kHz (indicated as dots on the amplitude stable branch in Fig. 10) and $\bar{y}=0.0209$, $D=0.03$. Small amplitude oscillation in time (a) and its autopower spectrum (b). Tapping mode response in time (c) and its autopower spectrum (d). In (d), tapping mode response generates the higher harmonics.

of periodic folds or global SN bifurcations[26] at points SN1, SN2, SN3, and SN4 in Fig. 10. Each bifurcation corresponds to the creation or the destruction of a pair of a stable (indicated by solid lines) periodic orbit and an unstable periodic orbit (indicated by dotted lines). This leads directly to the observed jumps and hysteretic behaviors in Fig. 2 because as a frequency sweep is performed in Fig. 10, the response follows a stable solution up to a bifurcation point where it jumps to another stable branch that lies in its basin of attraction.

Several observations can be made from the measured and computed results:

(i) The computed phase response along the ''saturated'' amplitude branch is slightly different from the experimentally measured response. This could arise because (a) the experimental phase measurement technique does not take into account the higher harmonics that are present on this branch, or (b) indicate the need for better tip-sample contact models. The present contact interaction is assumed to be perfectly elastic, suggesting that additional dissipative mechanisms during contact may need to be included to reproduce accurately the experimental phase response.

(ii) No period doubling bifurcation was detected on the saturated amplitude branch, for the chosen parameter values. At lower damping or higher forcing levels, this can occur leading to the generation of subharmonics in the response.[5,27]

(iii) Large-amplitude tapping and low-amplitude forced responses coexist for a range of excitation frequencies corresponding to the saturated amplitude branch (Fig. 10). For example, the time histories and autopower spectra of the two coexisting at excitation frequency at 46 kHz (Fig. 10) are plotted in Fig. 11. This demonstrates that the large-amplitude tapping solution clearly contains higher harmonics while the lower-amplitude solution is nearly purely harmonic. The large-amplitude resonant motions generate higher harmonics as the tip sharply taps the surface. Besides the higher harmonics, a significant zero-frequency component [Fig. 11(d)] is generated. The inherent quadratic nonlinearities in the at-

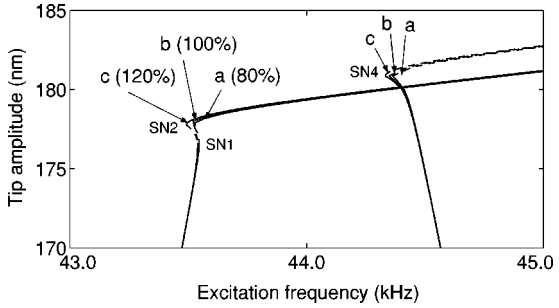


FIG. 12. Tapping amplitude responses due to variation of $C_1$. The cases $a,b,c$ indicate $C_1=6.04\times10^{-7}$ (80% of the nominal value), $7.55\times10^{-7}$ (nominal value), $9.06\times10^{-7}$ (120% of the nominal value), respectively. Solid/dotted lines indicate stable/unstable solutions, respectively. Tip amplitude refers to the peak-to-peak tip oscillation amplitude of the microcantilever.

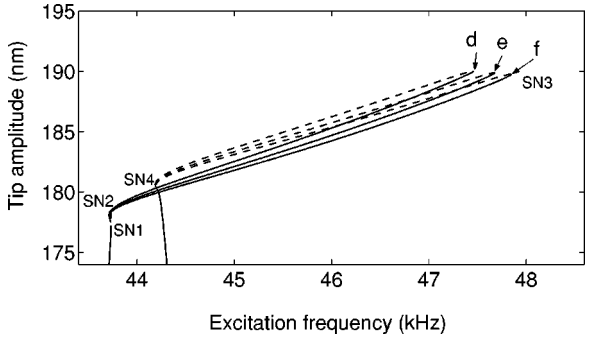


FIG. 13. Tapping amplitude responses due to variation of $C_2$. The cases $d,e,f$ indicate $C_2=3.64\times10^{2}$ (80% of the nominal value), $4.55\times10^{2}$ (nominal value), $5.46\times10^{2}$ (120% of the nominal value), respectively. Solid/dotted lines indicate stable/unstable solutions, respectively. Tip amplitude refers to the peak-to-peak tip oscillation amplitude of the microcantilever.

tractive van der Waals forces play an important role in the generation of the zero-frequency component.

### D. Sensitivity of the nonlinear response to parameter variations

The tip-sample interaction force $\overline{F_i}$ in Eq. (6) contains two normalized coefficients $C_1$ and $C_2$. $C_1$ is directly proportional to the product of Hamaker constant $A$ and tip radius $R$, and $C_2$ is directly proportional to the effective elastic modulus $E^*$. $C_1$ therefore is a measure of the van der Waals adhesion between the tip and sample and $C_2$ is a measure of the elastic indentation forces during contact. Because all the computation results use $C_1$ and $C_2$, which are calculated based on the values listed in Table I, it is useful to predict the sensitivity of the nonlinear response to a variation of tip-sample interaction parameters.

The computed responses in AUTO due to $\pm20\%$ perturbations of the original $C_1$ are shown in Fig. 12. Increasing $C_1$ clearly leads to larger adhesion and thus a greater softening nonlinear response prior to contact initiation. The ''hysteretic'' frequency range between bifurcations SN1 and SN2 is quite small for this specific tip-sample combination. In general, the extent of this range depends fundamentally upon the ratio of van der Waals forces to the cantilever elastic restoring forces just prior to contact initiation. For constant damping, tip-sample separation, and excitation amplitude, the greater the van der Waals forces compared to the spring stiffness force near the onset of contact, the greater the frequency range between SN1 and SN2. Specifically, for $C_1$ being 120% of its nominal value, the bifurcation point SN2 occurs at 43.45 kHz compared to 43.48 kHz for the nominal case. Therefore, for this specific cantilever located at the chosen distance from the sample, the sensitivity of the nonlinear response to variations in $C_1$ (or equivalently in the assumed Hamaker constant) is relatively small. This implies that the close correspondence between the theoretical prediction and experimental results in the region near SN1 and SN2 is quite robust.

It may be noted, however, that this sensitivity analysis is valid only for the specific cantilever located at the chosen distance from the sample. Because the system is highly nonlinear rapid changes can possibly occur in the shapes of potential wells as system parameters are changed. For example, if the cantilever is sufficiently soft, or if the adhesion is very high, a small change in the Hamaker constant could drive the system from region II to region I resulting in qualitatively different dynamics. Therefore, the parameter sensitivity of the nonlinear response of softer cantilevers or of cantilevers located closer to the surface is expected to be much greater than for the chosen case.

The computed nonlinear responses for $\pm20\%$ perturbations of the original $C_2$ are shown in Fig. 13. Increased $C_2$ leads to a greater extent of hardening nonlinear response following initiation of contact. Increased $C_2$ leads to a larger frequency range of the''saturated'' amplitude region and reduced slope of the tip amplitude with respect to the excitation frequency. The frequency range between SN3 and SN4 is affected by the elasticity of the sample. For softer samples, the potential well in the contact region [Fig. 7(c)] is shallower. Specifically, for $C_2$ being 120% of its nominal value, the bifurcation point SN3 occurs at 47.81 kHz compared to 47.55 kHz for the nominal case. Moreover, the slope with excitation frequency of the saturated amplitude response depends on the sample elasticity. For a rigid sample this slope is zero while for softer samples the slope increases. The computed responses in AUTO show that the perturbations in $C_2$ change the slope and length of the saturated amplitude branches. This indicates a greater sensitivity of the nonlinear response to variations in sample elasticity.

### E. Effects of parametric excitations

The tip-sample interaction term (especially van der Waals forces) in Eqs. (1) and (6) includes explicit time-dependent excitation $y(t)=Y\sin\Omega t$. This also leads to *parametric* excitation in addition to forced excitation of the microcantilever, an effect that is mostly ignored in the literature. Consider the excitation frequency to be far from the fundamental cantilever natural frequency. Because the tip amplitude and base excitation in this case can be assumed to be small compared to the tip-sample separation, the interaction force can be expanded in a Taylor series expansion as

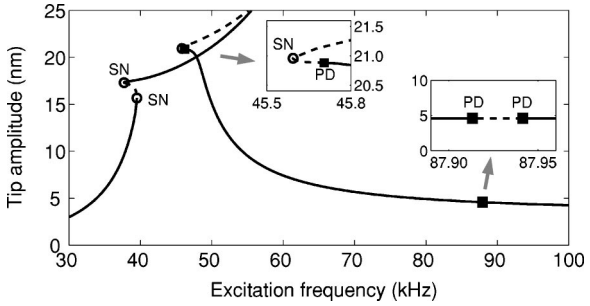


FIG. 14. Computed tapping mode response in AUTO with very high-$Q$ factor ($Q=1\times10^5$, $Z=10$ nm, $\bar{y}=0.1$). SN stands for a saddle-node or period-fold, and PD stands for a period-doubling bifurcation. Tip amplitude indicates the peak-to-peak tip oscillation amplitude of the microcantilever.

$$\bar{F}_i(\bar{z}) = C_1/\bar{z}^2 \quad \text{for} \quad \bar{z} > \bar{a}_0$$

$$= C_1/[1-\bar{\eta}(\tau)-\bar{y}\sin\bar{\Omega}\tau]^2$$

$$\approx C_1(1+2\bar{\eta}+2\bar{y}\sin\bar{\Omega}\tau+2\bar{\eta}^2+2\bar{y}^2\sin^2\bar{\Omega}\tau$$

$$+4\overline{\eta y}\sin\bar{\Omega}\tau+\text{h.o.t.}$$

Note that the leading-order nonlinearity is quadratic in nature and that external excitations occur at higher harmonics also. More importantly, the Taylor series expansion reveals the occurrence of the parametric excitation term $4\overline{\eta y}\sin\bar{\Omega}\tau$. The higher-order terms (h.o.t.) in the expansion also contain nonlinear parametric excitation terms. Parametric excitation leads to primary parametric instability when $\bar{\Omega}$ is close to twice the microcantilever fundamental frequency.[17,28] In the presence of additional external forcing, the effect of the parametric instability is to destabilize the forced periodic response in specific frequency ranges.

Parametric instability depends critically on the magnitude of parametric excitation relative to the modal damping.[28] Because the magnitude of parametric excitation depends on $C_1$, the parametric effects can be increased by increasing the van der Waals forces or by bringing the tip closer to the sample. Likewise, the modal damping is greatly reduced in vacuum AFM applications. This is demonstrated in Fig. 14 for the case of a tip located 10 nm from the sample with $Q=10^5$ with $\bar{y}=0.1$. It is observed that the primary parametric instability occurs at an excitation frequency close to twice the natural frequency (inset in Fig. 14). Numerical simulations of the response at an excitation frequency are shown just below the unstable range in the inset of Fig. 14 and in the stable range are shown in Fig. 15.

The primary parametric instability clearly occurs as a period doubling bifurcation that destabilizes the forced harmonic response of the microcantilever. A pair of period doubling bifurcations is also observed at large amplitudes in Fig. 14 (see inset for details) when $\bar{\Omega}$ is close to the fundamental natural frequency of the microcantilever. The occurrence of this pair of period doubling bifurcations just preceding contact with the sample can be due to both the effects of the nonlinear forced response as well as the secondary parametric resonance. Therefore, the consistent inclusion of the explicit time-dependent terms in the interaction force [Eqs. (1) and (6)] can lead to significantly different results for the stability of periodic motions of the microcantilever. These terms are especially important to include for vacuum AFM applications and/or for applications with large adhesion between the tip and sample.

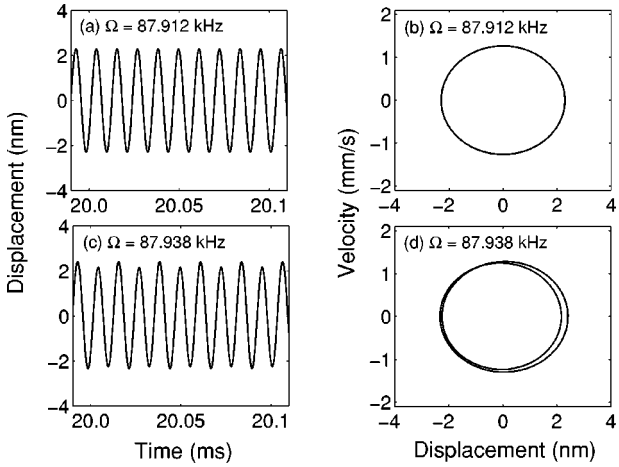


FIG. 15. Time responses and their phase portraits with near twice of the fundamental frequency of the microcantilever (a),(b) before the period-doubling bifurcation, and (c),(d) after the period-doubling bifurcation.

### F. Role of nonlinear system identification

The clear connection between the tip-surface interaction potential and the resulting nonlinear tip response as well as the sensitivity of the nonlinear response to variations in interaction parameters, suggest that nonlinear system identification techniques can be used to extract the tip-sample interaction parameters from the vibration response. This idea has also been suggested by Paulo and García.[15] A variety of techniques exist in the literature for the identification of nonlinear vibratory systems.[29–33] However, several unique features of the AFM microcantilever system preclude the application of many of the above techniques. The response of AFM microcantilever is strongly nonlinear in the tapping mode with multiple sources of nonlinearities and the presence of impacts with the sample. In the tapping mode, the input excitation in AFM microcantilever is purely harmonic. The tapping mode response as demonstrated in Fig. 11 contains a zero-frequency component in addition to higher harmonics. This suggests that harmonic-balance-based frequency domain analysis[29] of AFM data can lead to rapid and convenient estimation of the tip-sample interaction parameters such as the Hamaker constants and sample elasticity. It may be noted that harmonic-balance-based frequency-domain methods require an *a priori* prescription of the tip–surface interaction potential model and estimate directly the model parameters. This is a current area of research of the authors.

## V. CONCLUSIONS

The nonlinear dynamic response of diving board microcantilevers interacting with samples in tapping mode AFM

are investigated computationally as well as experimentally. A range of observed nonlinear behavior in experiments such as jumps and hysteresis in amplitude and phase response can be explained quantitatively from nonlinear dynamical systems theory. Specifically, the presence of softening-hardening nonlinearities are directly correlated to the asymmetric single-well potential between the tip and sample. The nonlinear response depends sensitively on the interaction parameters as well as on the forced and parametric excitation terms. The results also suggest strongly that nonlinear system identification methods could accurately extract from tapping mode vibration data quantitative estimates of the tip-sample interaction parameters.

## ACKNOWLEDGMENTS

The corresponding author (A.R.) acknowledges the support of the National Science Foundation (NSF) under Award No. 0116414-CMS. Dr. Alison Flatau is the program manager. One of the authors (R.R.) would like to thank Professor Julio Gómez-Herrero and Professor Jaime Colchero for their continued help with the NanoTec™ $WS\times M$ software.

[1] A. Kühle, A.H. Sørensen, J.B. Zandbergen, and J. Bohr, Appl. Phys. A: Mater. Sci. Process. **66**, S329 (1998).
[2] R. García and A.S. Paulo, Phys. Rev. B **60**, 4961 (1999).
[3] P. Gleyzes, P.K. Kuo, and A.C. Boccara, Appl. Phys. Lett. **58**, 2989 (1991).
[4] A. Kühle, A.H. Sørensen, and J. Bohr, J. Appl. Phys. **81**, 6562 (1997).
[5] W. van de Water and J. Molenaar, Nanotechnology **11**, 592 (2000).
[6] M.V. Salapaka, D.J. Chen, and J.P. Cleveland, Phys. Rev. B **61**, 1106 (2000).
[7] N.A. Burnham, O.P. Behrend, F. Oulevey, G. Gremaud, P.-J. Gallo, D. Gourdon, E. Dupas, A.J. Kulik, H.M. Pollock, and G.A.D. Briggs, Nanotechnology **8**, 67 (1997).
[8] N.A. Burnham, R.J. Colton, and H.M. Pollock, Nanotechnology **4**, 64 (1993).
[9] M. Marth, D. Maier, J. Honerkamp, R. Brandsch, and G. Bar, J. Appl. Phys. **85**, 7030 (1999).
[10] L. Nony, R. Boisgard, and J.-P. Aimé, Eur. Phys. J. B **24**, 221 (2001).
[11] M. Gauthier, N. Sasaki, and M. Tsukada, Phys. Rev. B **64**, 085409 (2001).
[12] D. Sarid, *Scanning Force Microscopy: With Applications to Electric, Magnetic and Atomic Forces* (Oxford University Press, New York, 1991).
[13] O.P. Behrend, L. Odoni, J.L. Loubet, and N.A. Burnham, Appl. Phys. Lett. **75**, 2551 (1999).
[14] X. Chen, M.C. Davies, C.J. Roberts, S.J.B. Tendler, P.M. Williams, and N.A. Burnham, Surf. Sci. **460**, 292 (2000).
[15] A. San Paulo and R. García, Phys. Rev. B **64**, 193411 (2001).
[16] H. Hölscher, W. Allers, U.D. Schwartz, and R. Wiesendanger, Phys. Rev. Lett. **83**, 4780 (1999).
[17] A. H. Nayfeh and D. T. Mook, *Nonlinear Oscillations* (Wiley, New York, 1979).
[18] B.V. Derjaguin, V.M. Muller, and Y.P. Toporov, J. Colloid Interface Sci. **53**, 314 (1975).
[19] J. Israelachvili, *Intermolecular and Surface Forces* (Academic Press, San Diego, 1992).
[20] The stability can be determined by examining the sign of the second derivative of the total potential energy (sum of the cantilever elastic energy and the interaction potential) evaluated at that equilibrium.
[21] U. Rabe, K. Janser, and W. Arnold, Rev. Sci. Instrum. **67**, 3201 (1996).
[22] L. Meirovitch, *Principles and Techniques of Vibrations* (Prentice-Hall, Upper Saddle River, NJ, 1997).
[23] The approximate eigenfunctions are derived using a Galerkin approximation as a finite sum of the eigenfunctions of a clamped-free microcantilever: $\Phi_i(x)=\Sigma_{j=1}^{N} v_j \psi_j(x)$, where $v_j$ are the components of the eigenvector in the linearized eigenvalue problem and $\psi_j(x)$ are the orthogonal eigenfunctions of a clamped-free microcantilever.
[24] $\overline{y}=0.020\,90$ means that the dither excitation amplitude is assumed to be 2.09% of the equilibrium gap (90 nm) or $\approx$1.9 nm To verify this, the RMS amplitude at the *base* of the cantilever was measured (with poor signal-to-noise ratio) in the resonance range to lie between 1–3 nm.
[25] E. J. Doedel, A. R. Champneys, T. F. Fairgrieve, Y. A. Kuznetsov, B. Sandstede, and X. Wang, AUTO97: *Continuation and Bifurcation Software for Ordinary Differential Equations* (Concordia University, Montreal, Canada, 1997).
[26] J. Guckenheimer and P. Holmes, *Nonlinear oscillations, dynamical systems and bifurcations of vector fields* (Springer Verlag, New York, 1991).
[27] N.A. Burnham, A.J. Kulik, G. Gremaud, and G.A.D. Briggs, Phys. Rev. Lett. **74**, 5092 (1995).
[28] D. W. Jordan and P. Smith, *Nonlinear Ordinary Differential Equations: An Introduction to Dynamical Systems*, 3rd ed. (Oxford University Press, New York, 1999).
[29] K. Yasuda and K. Kamiya, ASME Trans. J. Appl. Mech. **64**, 275 (1997).
[30] S.F. Masri and T.K. Caughey, ASME Trans. J. Appl. Mech. **46**, 433 (1979).
[31] E.F. Crawley and A.C. Aubert, AIAA J. **24**, 155 (1986).
[32] R.W. Krauss and A.H. Nayfeh, Nonlinear Dyn. **18**, 69 (1999).
[33] K. Worden and G. R. Tomlinson, *Nonlinearity in Structural Dynamics: Detection, Identification and Modelling* (Institute of Physics, University of Reading, Berkshire, 2001).